JOURNAL OF Applied Polymer SCIENCE

Effects of Annealing on Structure and Deformation Mechanism of Isotactic Polypropylene Film with Row-Nucleated Lamellar Structure

Zhitian Ding, Ruiying Bao, Bo Zhao, Jing Yan, Zhengying Liu, Mingbo Yang
State Key Laboratory of Polymer Materials Engineering, College of Polymer Science and Engineering, Sichuan University, Chengdu, Sichuan, China
Correspondence to: Z. Liu (E-mail: liuzhying@scu.edu.cn) or M. Yang (E-mail: yangmb@scu.edu.com)

ABSTRACT: The effects of annealing on structure and deformation mechanism of isotactic polypropylene films with row-nucleated lamellar structure were investigated. The microstructure developments of the lamellar structure and amorphous during annealing were detected by differential scanning calorimeter and Fourier transform infrared. As annealing went on, the "core–shell sandwich" lamellar structure was proposed to explain the unique tensile property and the microstructure changes of the annealed films. The recrystallized lamellar structure improved the ability of slipping resistance of original lamellar structure during stretching. Microporous membranes were produced through melt extrusion/annealing/uniaxial stretching way. The uniformities of micropore structure of microporous membranes were improved as the annealing time increased for the annealed films. As the "core–shell sandwich" structure developed during annealing, the shapes and diameters of micropore structure were getting more uniform. The annealing time for annealed films improved the water vapor transmission of the microporous membranes, indicating the increased interconnectivity of the pore structure. The pore dimensions of the microporous membranes measured by mercury porosimetry increased with the annealing time for annealed films. © 2013 Wiley Periodicals, Inc. J. Appl. Polym. Sci. 130: 1659–1666, 2013

KEYWORDS: porous materials; properties and characterization; films

Received 31 December 2012; accepted 25 March 2013; Published online 3 May 2013
DOI: 10.1002/app.39351

INTRODUCTION

For semi-crystalline polymer, the annealing is performed at a certain temperature (T_α) which activates the mobility of the crystalline structure.[1] Annealing plays an important role in improving performances by eliminating the internal stress and defects of products. After processing, a portion of the polymer chains in the crystalline region and amorphous are not in a thermodynamic equilibrium state. Polymer chains could adjust their energy state to the equilibrium state as the mobility of chains increase during annealing procedure. The chains in the imperfect crystalline region will rearrange themselves into a more perfect crystalline structure and the defects will be eliminated. If the polymer chains deformed to induce orientation during processing, the chains in the oriented amorphous region often alter their oriented conformation into a more random coiled configuration during the annealing process.[2] The important influencing factors of annealing on the structure changes of samples include annealing temperature, time, and tension. At the same time, the effects of the prior physical state of samples (such as oriented or unoriented) as well as processing thermal history of samples, chemical architecture of polymer chains, and polymer resin composition (molecular weight, degree of branching, etc.)[3] on the structure of the samples during annealing process should be considered.

Microporous membranes are widely used in many fields such as sewage purification, battery separator, and extraction. Owing to the wide range of chemical structures, optimum physical properties, and low cost, polymers and polymer blends are reliable materials for producing microporous membranes. There are several techniques usually used for the fabrication of the microporous membranes, and most of them are based on solution casting process (wet process) and melt extrusion/annealing/uniaxial stretching (MAUS) way (dry process). Solution casting produces the microporous membranes through solvent evaporation followed by phase separation, but the obvious drawbacks, difficult recycle of solvent and the solvent contamination, are inevitable.[4] No solvent was used to make MAUS cost less and be more environmentally friendly. Both the pore shape and the tensile strength of the uniaxially stretched microporous membranes made from MAUS way were highly oriented through machine direction (MD), since the film was stretched only in MD. Significant difference between the MD and transverse direction (TD) strengths may result in a splitting problem.[5]

The unique row-nucleated lamellar structure endows the high oriented films with "hard-elastic" character,[6–14] which facilitates the preparation of the microporous membranes through MAUS way.[15–21] Annealing is one of the important procedures of MAUS way and plays a critical role in the microporous membrane production. During annealing procedure, the lamellar thickness increases and the lamellar orientation and uniformity are improved,[12] companied with the removing of the defects in the crystalline structure. Some researchers found that the efficient annealing time for polypropylene precursor films was 10 min at 140°C, and beyond that, the orientation and crystallinity of the films remained constant.[14] Annealing is always considered an indispensable procedure during the preparation of the microporous membrane, but how the structures of the films develop during the annealing is still completely unclear. Moreover, the effect of the annealing on the micropore forming of the follow-up stretching is not yet investigated particularly.

The developments of oriented lamellar structure and amorphous in precursor films during annealing for precursor films often have important effects on properties or performance of annealed films in the next usage or application (such as mechanical property, micropore forming property in the preparation of the microporous membrane made through MAUS way). So the quantitative analysis about the relationship between structural changes (crystallinity, orientation of chains in crystalline and amorphous) and exact one of the factors (annealing temperature, time and etc.) in the annealing procedure is important.

Among the semi-crystalline polymers, polyethylene and polypropylene were the general raw material for the fabrication of microporous membranes through MAUS way. Compared to polyethylene, polypropylene exhibited higher melting point, higher chemical resistance, and more excellent mechanical properties. Polypropylene had been selected as the raw material for making battery separator used microporous membranes through MAUS for more than 20 years.[4,5] In this work, the polypropylene was selected as the raw material for making microporous membranes. The temperature 140°C was often chosen as the annealing temperature in the existing researches for the preparation of the microporous through MAUS way.[15–21] In order to decrease the structural change rate for accurate detecting, in this research 135°C was chosen as the annealing temperature. The polypropylene precursor films with row-nucleated lamellar structure were annealed in a temperature-controlled chamber at 135°C for different times. The investigation for the annealing is limited in the dynamics problems of the structural changes. The crystallinity and orientation of the annealed films for different annealing times were detected using differential scanning calorimetry (DSC) and Fourier transform infrared (FTIR). FTIR was chosen because the chain orientation of both crystalline and amorphous region can be detected. The variation trends of crystallinity and orientation of the annealed films were obtained. The tensile properties of annealed films with different annealing times were tested through universal testing machine, and the unique strain–stress behaviors of annealed films for different annealing times were obtained. The annealed films with different annealing times were cold and hot stretched to form micropore structure to investigate the relationship of annealing time-crystalline structure-micropore forming. The water vapor transmission (WVTR) and pore dimensions of the microporous membranes were obtained. The results indicated the structural changes during annealing increased the interconnectivity of the pore structure and improved the pore size. To interpret the relationship between the annealing time, structural changes, tensile properties of the annealed films, and the micropore structure changes, a model named "core–shell sandwich" of crystalline structure development under annealing process was proposed.

EXPERIMENTAL

Material and Preparation of Isotactic Polypropylene Precursor Films

An extrusion grade of isotactic polypropylene (iPP, PP5341E1, ExxonMobil, MFR (melt flow rate) 0.05 g 10 min^{-1}) with weight average molecular weight (M_w) of 535.7 kg mol^{-1} and molecular weight distribution of 3.87 was used. The molecular parameters were measured by a gel permeation chromatography (PL-GPC200) at 150°C, with 1,2,4-trichlorobenzene as a solvent. The precursor film was extruded through a single screw extruder (D = 30 mm, L/D = 34, where D is the diameter of the screw, and L is the length of the screw) equipped with slit die of 1.25 mm thick and 400 mm width. The temperature settings of the extruder were 170°C, 200°C, 230°C, 240°C, and 235°C along the barrel from hopper to die, and the rotation speed of the screw was 40 rpm. A temperature-controlled chill roll with roll temperature of 25°C was equipped at the distance of 15 cm to the die exit. Two air knives were equipped to release compressed gas to the film surface right at the exit of the die. From the former work, the orientation of the crystalline phase in precursor film must be greater than 0.5 for preparing microporous membranes from iPP through MAUS way. High draw ratio and high cooling for polymer melt at the exit of the die was beneficial to make crystalline phase oriented. The processing parameters in this work were the optimized condition in our experimental condition. The processing parameters for the preparation of precursor films could be also found in the former work.[22] The row-nucleated lamellar crystalline structures of precursor films would be formed by applying elongation stress and intensive cooling on the film surface right at the exit of the die.[16–18,20,22] The degree of melt extension was described as draw ratio, DR = V_2/V_1, where V_1 is the velocity of melt outflow from die exit, and V_2 is the linear velocity of rotation of take-up roll. DR = 60 was used for manufacturing of the precursor films. The thickness of the precursor films was 21 μm.

The precursor films were annealed in a temperature-controlled chamber at 135°C for 0 s, 20 s, 40 s, 60 s, 120 s, 180 s, 240 s, 300 s, 420 s, 480 s, 600 s, 780 s, 960 s, and 1140 s, respectively. After annealing procedure, the annealed films were immediately dipped into liquid nitrogen for freezing the lamellar structure. A Shimadzu AGS-J universal testing machine equipped with a temperature control chamber was used for the stretching of the annealed films. To evaluate the effects of lamellar structure developments during annealing on tensile and micropore forming properties of the annealed films, the annealed films were stretched and heat fixed according to the following procedures.

The annealed films were stretched to 40% of initial length at 25°C using the speed of 60 mm min^{-1} and subsequently were stretched to 40% of initial length at 130°C using the speed of 15 mm min^{-1}. Cold stretching lead to lamellar separation and pore creation, while hot stretching leads to pore elongation. Finally, the stretched films were heat fixed at 130°C for 10min. The final microporous membranes with annealing time 20 s, 40 s, 240 s, etc., were named as M20, M40, M240, etc.

Differential Scanning Calorimetry

The crystallization behaviors of the specimens before and after annealing were analyzed using TA Q20 differential scanning calorimeter under a nitrogen atmosphere. The samples were heated from 0°C to 190°C at a heating rate of 10°C min^{-1}. The crystallinity of the specimens was calculated from enthalpy change values obtained in the heating curve, supposing a heat of fusion of 209 J g^{-1} for fully crystalline polypropylene.[23]

Fourier Transform Infrared

For FTIR measurements, a Nicolet 6700 FTIR instrument from Thermo Electron Corp. was used. The beam was polarized through a Spectra-Tech zinc selenide wire grid polarizer from Thermo Electron Corp. The measurement is based on the absorption of infrared light at certain frequencies corresponding to the vibration modes of atomic groups present within the molecule. In addition, if a specific vibration is attributed to a specific phase, the orientation within that phase can be determined.[16–18,20] If the films are oriented, the absorption of plane-polarized radiation by a vibration in two orthogonal directions, specifically parallel and perpendicular to a reference axis machine direction (MD), should be unequal. The ratio of these two absorption values is defined as the dichroic ratio, D. So the value of D can be obtained from the equation $D = A_{||}/A_{\perp}$,[22] where $A_{||}$ and $A_{\perp}$ are the absorption parallel and perpendicular to MD, respectively. The Herman orientation function (f) of this vibration is obtained according to $f = (D - 1)/(D + 2)$.[22] For polypropylenes, absorption at the wavelength of 998 cm^{-1} is attributed to the crystalline phase (c-axis), while absorption at the wavelength of 972 cm^{-1} is due to the contribution of both crystalline and amorphous phases. From the former absorption, the orientation of the crystalline phase (f_c) can be determined, while from the latter, the average orientation function (f_{av}) is obtained. The orientation of the amorphous phase (f_{am}) can be calculated according to $f_{av} = X_c f_c + (1-X_c) f_{am}$, where X_c is the degree of the crystallinity calculated from DSC. Using FTIR, the global crystalline and amorphous orientations can be determined.

Scanning Electron Microscopy

Scanning electron microscopy (SEM) observations for the surface morphology of the etched film and the membranes were carried out using a scanning electron microscope (Inspect F, FEI). All samples were coated with a thin layer of gold/palladium alloy before the tests.

Porosimetry and WVTR

The pore size distribution and porosity of the membranes were measured using a mercury porosimeter (AutoPore IV 9500, Micromeritics Instrument Corp). After the cell was evacuated, it was filled by mercury, and then pressure was applied to force mercury into the pore structure of the microporous membranes. The amount of intruded mercury was related to the pore size and porosity. Permeability of water vapor was measured via a Permatran-W (W3/330, Labthink) at 25°C. The test sample area was 10 cm^2 for all samples.

RESULTS AND DISCUSSION

Effects of Annealing on Orientation Structure and Crystallinity of Precursor Films

The precursor films were produced using film casting. The resin and processing conditions (DR, cooling condition, roll temperature) were chosen for producing precursor films with highly oriented lamellar structure.[22] The drawing flow in the casting process made the polymer melt to produce numerous oriented nuclei which can induce oriented row lamellar structure to form row-nucleated lamellar structure.[24–26] Annealing of precursor films was performed in a temperature-controlled chamber at 135°C for different times. The changes of the chain orientation in crystalline region (f_c) and amorphous region (f_{am}) and crystallinity (X_c) of annealed films with the increase of annealing time are shown in Figure 1. It was obvious that the rapid increases of f_c, f_{am}, and X_c with the annealing time mainly took place in 40 s and basically tended to level off until 200 s. In the first 40 s, f_c, f_{am}, and X_c of annealed films were 12%, 8%, and 10% higher than the precursor films. As the annealing proceeded for 200 s, f_c, f_{am}, and X_c of annealed films were 15%, 12%, and 13% higher than the precursor films. During annealing time of 200–600 s, the f_c, f_{am}, and X_c increasing rate was less than 2%. But when annealing time was from 600 s till 1140 s, the f_c, f_{am}, and X_c increased again at a lower growth rate than the first 40 s. At the end of the annealing, the f_c, f_{am}, and X_c of annealed films were 17%, 14%, and 18% higher than the precursor films. The three character factors' variation of the annealed films showed a similar trend. But the effect of annealing on f_c is apparently more significant than f_{am}. More details about the structure development of the crystalline region and amorphous region will be discussed in the latter sections.

To detect the changes of the crystalline structure, the annealed films with different annealing times were tested by DSC, and the results are shown in Figure 2. As the annealing time increased, the position of main peak of the precursor films is

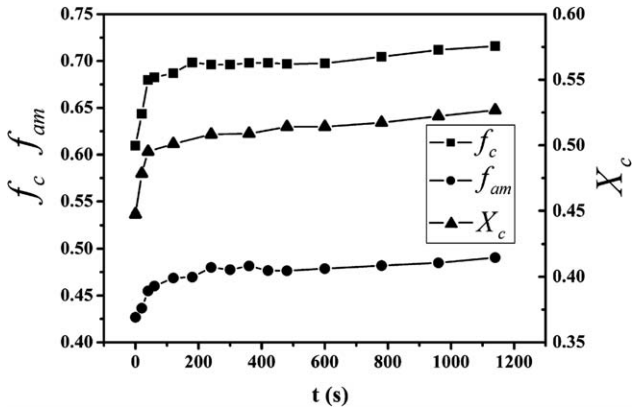

Figure 1. Changes of the orientation parameters (f_c and f_{am}) and the crystallinity (X_c) with the increasing of annealing time.

Applied Polymer SCIENCE

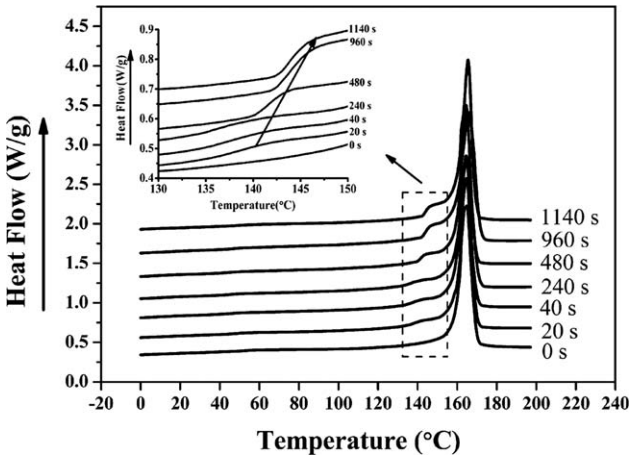

Figure 2. DSC curves of annealed film with different annealing times.

nearly unchanged, suggesting that the crystal lamellar thickness of the precursor films did not change much with the increasing annealing time. The significant changes were that there is a shoulder peak emerge around 140°C for the annealed films, which has also been reported by other authors.[16,27] In this work, the position of the shoulder peak shifted from 141°C of the films experiencing 20 s of annealing process to 146°C of the one experiencing 960 s of annealing process. The area of the shoulder peak grew with the increasing the annealing time. It can be supposed that the structure corresponding to the shoulder peak should take responsibility for the crystallinity growth of the annealed films. According to the Thomson–Gibbs formula,[28–30] the temperature of the DSC peak position one-to-one corresponded to the lamellar thickness. Higher melting temperature meant thicker lamellar structure. The presence of the shoulder peak corresponded to a kind of newly formed lamellar structure during annealing, and the position shift of the shoulder peak indicated that the newly formed lamellar structure became thicker as the annealing went on. The reason for this argument will be discussed in the latter chapter.

Deformation Behaviors of the Precursor Films with and Without Annealing

The stress–strain behaviors of the annealed films with different annealing times were shown in Figure 3 (the dotted area is blown up as the inset image). All samples exhibited hard-elastic behavior and showed distinct yield point, which were different from the samples with spherulitic structure.[31,32] The initial linear part of curve OA corresponded to the elastic deformation of the films until the yield point (yield stress σ_y). As the annealing time increased, the σ_y and elastic modulus of the annealed films dramatically reduced. The elastic modulus in this area was dominated by amorphous regions in the films where the tie chains bear the main load.[31] The increase of X_c of the annealed films during annealing means the decrease of amorphous regions, so the σ_y and elastic modulus of the annealed films reduced as the annealing time increased. The major decrease of the σ_y and elastic modulus of the annealed films took place in the first 40 s during annealing. As the annealing went on, the σ_y and elastic modulus of the annealed films maintained in a certain level. This phenomenon was directly related to the changes of f_c, f_{am}, and X_c of annealed films during annealing. After yielding, there was a short intermediate process AB for all samples with same slope tan α_1. After the uniform elastic deformation area of OA, the deformation mode of the curve was transformed into elastic and plastic deformation modes. AB was the transition from the uniform elastic deformation mode of first part OA to another deformation mode involving both elastic and plastic components.[31] After this process, the profile of the curves behaved with very different types for annealed films and unannealed films. For all annealed films, the curves of BCD had two stages, the first one BC with slope tan α_2 and the second one CD with slope tan α_3. The separation of lamellar structure and the formation of "bridging structure" (the fibrous structure between separated lamellae)[13,33] between the lamellar structure are responsible for the stress increase in the stage BC of deformation for the annealed films.[12,34] Until a limit of the lamellar separating in a large strain, the lamellar structure would collapse, slip, and turn into oriented fibrous structure, while the stress–strain curve switches from the stage BC into the stage CD of deformation for the annealed films. By contrast, for the unannealed film, the curve of BCD was almost with one same slope tan α_3. Thus, it can be seen that the crystal and amorphous structure changes originating from the annealing had a great effect on the deformation behaviors of the films.

Effects of Annealing on Micropore Forming of Annealed Films

Microporous membranes were made from annealed films following the procedures mentioned in the "Experimental" section. The surface morphologies of all the samples were observed by SEM, and the results are shown in Figure 4. From Figure 4(a–f), apparently, the uniformities of micropore shape, micropore diameter, and lamellar spliting of the samples were improved as the annealing time increased. In Figure 4(a), the domains of micropore forming were uneven, and the size of micropores was nonuniform. Most part of the lamellar structure separated in a low degree. As the precursor film was annealed for a short time, the lamellar structure was imperfect and the amorphous was tough. The lamellar structure twisted, bended, and even slipped under the pulling of the "bridging structure,"

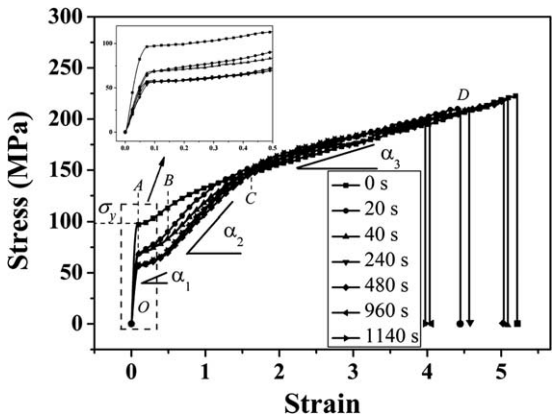

Figure 3. Stress–strain curves of annealed films with different annealing times; the dotted area is blown up as the inset image.

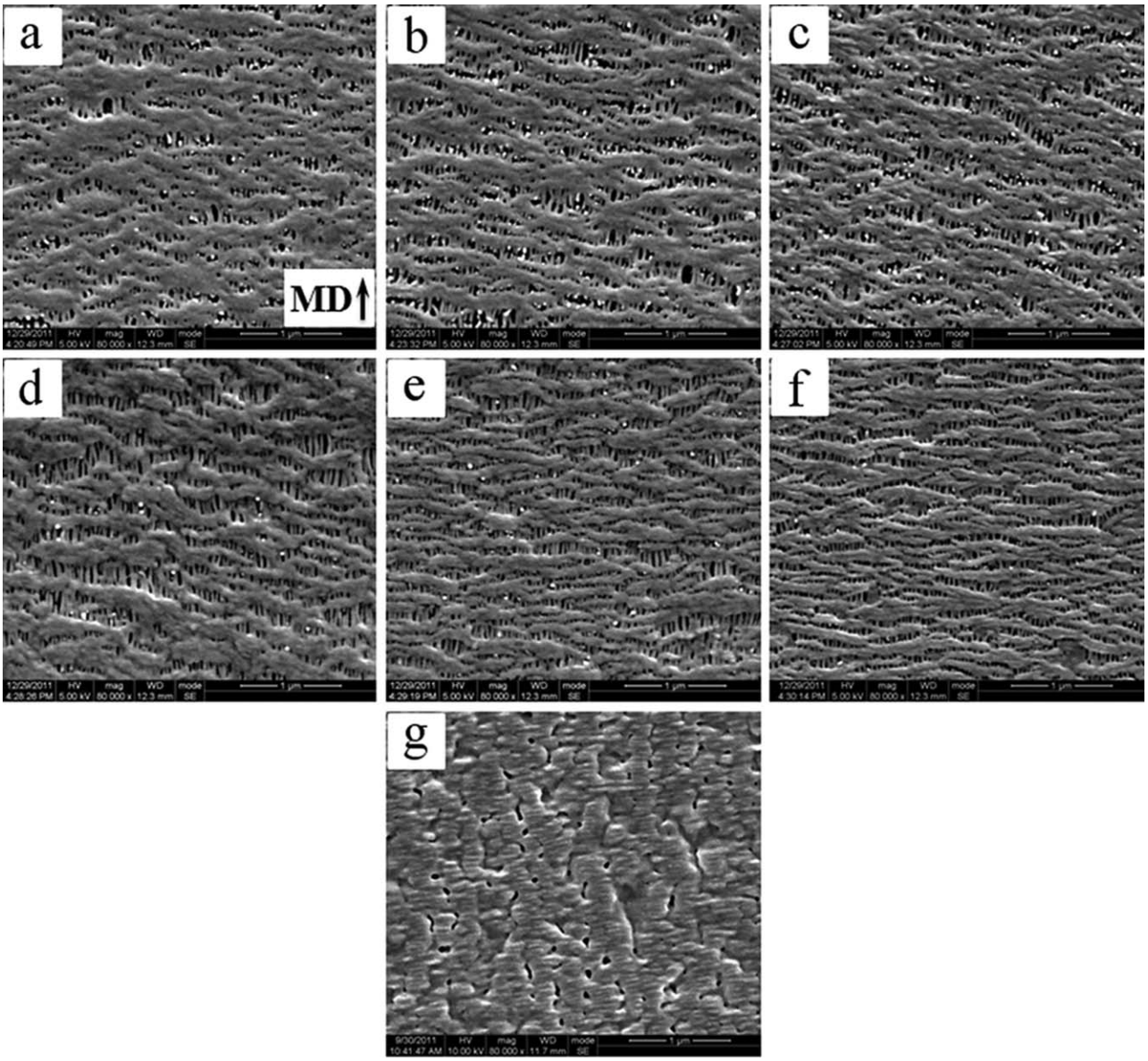

Figure 4. SEM images of surface morphology of microporous membranes from annealed films with different annealing times (a: M20, b: M40, c: M240, d: M480, e: 960s, f: M1440) and microporous membrane from unannealed film (g: M0); annealing was performed at 135°C; DR (draw ratio) = 60, cold stretching of 40% followed by hot stretching of 40%.

so the micropores appeared in a nonuniform form. As the annealing time increased, the number and size of micropores increased obviously in M40 and M240 [Figure 4(b,c)], and the domains of micropore forming were more uniform as well. But the twisting and bending degrees of lamellar structure still existed. As the annealing time increased for M480 [Figure 4(d)], uniformities of micropore shape and micropore diameter improved much better than that of the M20 and M40. Dramatically, as the annealing time increased for M960 [Figure 4(e)], the micropore structure improved further than that shown in Figure 4(a)–(d). The size of the micropores was uniform and the domains of micropore forming were homogenous. The lamellar structure's twisting and bending were greatly restrained. The most part of deformation mode for lamellar structure was separation instead of slippage. As the annealing went on for M1140 [Figure 4(f)], the uniformities of micropore shapes, micropore diameter, and areas of micropore forming were the best of all samples; the lamellar structure's twisting and bending were minimized. Each pore had almost the same size and sharp. The lamellar structure was barely twisted and perfectly oriented through MD. The 1140 s was the optimum time for this experiment annealing time region. The effect of annealing on the structure developments in a short time was the focus of this research.

In contrast, the surface morphology of membrane made from unannealed film M0 is shown in Figure 4(g). Under the stretching procedure, the surface morphology was distinct from the

Applied Polymer SCIENCE

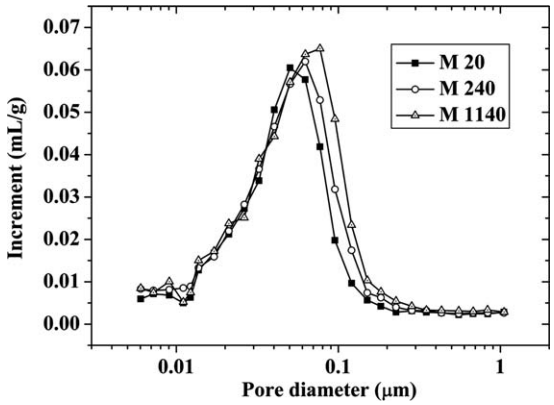

Figure 5. Pore size distribution for microporous membranes from annealed films with different annealing times; annealing was performed at 135°C; DR = 60, cold stretching of 40% followed by hot stretching of 40% (curves of M40, M480, and M960 are not shown in the figure, because M40 is similar to M240, and M480 and M960 were similar to M1440).

annealed samples. Few deformity micropores were found in the image. Interestingly, after 80% stretching rate, there were many highly oriented lamellar structure through MD found in the surface morphology. The lamellar structure could not be the original lamellar structure of the precursor film. Without annealed, the original lamellar structure would slipped into oriented fibrous structure through MD, then the chains in the oriented fibrous structure would fold themselves into lamellar structure.[35]

From above all, the annealing played the decisive role in forming the micropore structure through MAUS way. Although the micropore could be formed as the precursor films were annealed for a short time, the micropore structure was defective such as nonuniform micropore shapes and uneven micropore diameter. Nevertheless, as the annealing time was long enough, the shapes and diameters of micropore structure were getting more uniform. The increasing f_o, f_{am}, and X_c of annealed films were beneficial to micropore forming and prevented the lamellar structure from twisting, bending, or slipping during the stretching stages. The morphologies of the microporous membranes well corresponded to the results in Figures 1 and 2. The X_c of 480 s annealed film was the end of the quick growth stage. The shoulder peak of DSC curve for 480 s annealed film moved toward high temperature for 4°C, and after that, the shoulder peak movement was 2–3°C. In this experimental condition, at annealing temperature 135°C, 480 s was the shortest annealing time to obtain microporous membranes with better micropore structure.

Mercury Porosimetry and Permeability

The pore size distribution curves for microporous membranes from annealed films with different annealing times are shown in Figure 5. The curves of M40, M480, and M960 are not shown in the figure because M40 was similar to M240, and M480 and M960 were similar to M1440. It was obviously that the annealing time influenced the peak position of the pore size distribution curves and the peaks of the samples changed from 0.05 into 0.08 μm with the increasing annealing time. The area under the curves corresponding to the porosity of the membranes also increased with the annealing time. The lower porosity of the membrane with short annealing time was attributed to fewer pores' structure due to the little separation and more slippage of lamellar structure during stretching procedure. The structure developing of lamellae during annealing would dramatically influence the lamellar deformation behavior during stretching procedure. In Figure 4, the annealing time had great influence on the shapes of the micropores more and less influence on the pore size. The difference between M40 and M240 was slight. As the annealing time increased, the pore shapes of M480, M960, and M1140 improved. The porosity of samples is shown in Table I. The M480, M960, and M1140 had the similar porosity. The similar porosity corresponded to the similar pore size distribution curves. The porosity and pore size distribution curves of the M40 and M240 were also similar.

Table I. Properties of Microporous Membranes (Thickness = 16 μm)

Samples	Porosity	Pore diameter (μm)	Permeability of final membranes (g m^{-2} day^{-1}) (±10% error)
M20	0.31	0.05	7700
M40	0.34	0.06	8300
M240	0.35	0.06	10,200
M480	0.38	0.08	16,500
M960	0.38	0.08	15,900
M1140	0.38	0.08	15,700

Annealing was performed at 135°C; DR = 60, cold stretching of 40% followed by hot stretching of 40% (values are averaged over five tests for each sample).

The permeability of the microporous membranes was measured by water vapor. Water vapor permeability was performed under atmospheric condition with no pressure applied. Table I reports the water vapor permeability for the microporous membranes. The permeability results were in accordance with the pore size distribution results in Figure 5. The permeability was determined by both the pore size and pore interconnection. M20 and M40 with short annealing time had more lamellar slippage which would obstruct the through-pore forming and reduce the pore interconnection. In addition, smaller pore diameter would reduce the WVTR rate for the membranes with short annealing time. At the annealing temperature 135°C, the annealing time more than 480 s was necessary to obtain the better permeability and pore structure of the microporous membranes.

Model of Structural Developments of Films During Annealing

Throughout the highly cold and stretching processing during the preparation of precursor films, the polymer chains in the melt would fold themselves in the lamellar structure. The flaws of the chain structure and the entanglement points would affect the length of chain folding.[36] Many tie chains, tail chains, and loop chains would locate through the crystal regions and

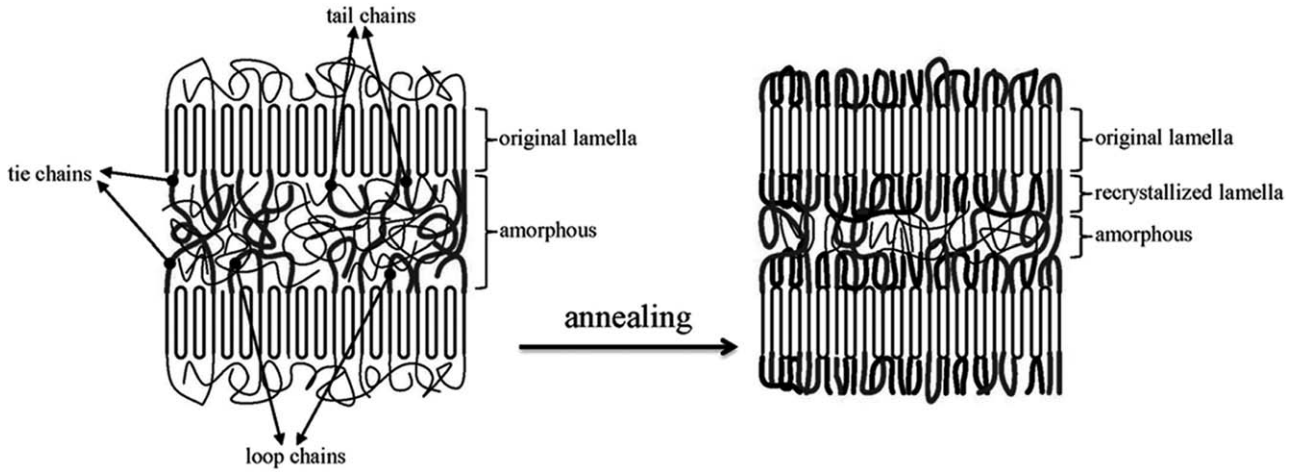

Figure 6. Sketch of the structure developing of lamellae during annealing.

amorphous regions. These chains would entangle with the each other in the amorphous. In the interface of the crystal-amorphous region, numerous polymer chains were in a certain stage of preordering. Once the annealing happened, the mobility of the polymer chains in the amorphous immediately increased. Most part of the crystallinity growth possibly occurred in the crystal-amorphous interface during annealing. The sketch of structure developing of lamellae during annealing is shown in Figure 6. The left part was the morphology of lamellar structure and amorphous before annealing, and the right part was the morphology of lamellar structure and amorphous after annealing.

When annealing began, the partly oriented tie chains, tail chains, and loop chains (Figure 6, left) would rearrange themselves and induce the nearby amorphous chains to recrystallize (Figure 6, right), which could be confirmed by the presence of the shoulder peak shown in the DSC curves in Figure 2. The shoulder peaks shifted from 141°C to 146°C, meaning that the recrystallized lamellae became thick in the chains' direction as the annealing went on. The thickness of original lamellae corresponding to main peak of the DSC curves was unchanged during annealing due to the chains had been fixed in the crystal lattice. The recrystallized lamellae tended to cling to the original lamella. In the edge of the recrystallized lamellae close to the amorphous, the chains had the mobility to rearrange themselves into the crystal lattice during annealing. At last, the thickness of the recrystallized lamellae increased as the annealing went on.

The growth of recrystallized lamellae would make the tie chains and tail chains oriented along the original lamellae. This would bring out the stretching of tie chains and tail chains which affected the orientation of the amorphous. The orientation increase of amorphous accorded with model in Figure 6. But the orientation increase of crystalline region was not clearly shown because the new recrystallized lamellae maintained the orientation stage exactly as the original lamellae. From Figure 1, it was observed that the growth trend of f_c, f_{am}, and X_c was the same. Maybe the reason for the orientation increase of the crystalline region was that the new recrystallized lamellae with the stretching of tie chains would push the original lamellae toward the middle of two layers of amorphous. The rearrangement in machine direction brought out the crystalline region orientation improvement.

The microstructure developments endowed the annealed films with unique mechanical properties. In linear elastic deformation area, the σ_y and elastic modulus of the annealed films were dominated by amorphous regions in the films where the tie chains bear the main load. The annealing brought out the ratio adjustment of the crystalline region and amorphous. With the decrease of the content of amorphous, the σ_y and elastic modulus of the annealed films decreased as the annealing went on. After linear elastic deformation area, the strain–stress curve of unannealed precursor film immediately switched into growth with one slope tan α_3. Before the growth with the slope tan α_3, the strain–stress curves of the annealed films grew with a higher slope tan α_2. The significant difference between them must result from the microstructure changes from the annealing. As Figure 3 shows, the effects of annealing on stress–strain curves were intensified as the annealing time increased. It was obvious that the tensile properties, f_c, f_{am}, and X_c of the annealed time were related.

As the annealing went on, the deformation mode of the lamellar structure transformed from twisting, bending, and even slippage into separation. Only after the recrystallized lamellae clinged to original lamellar structure during the annealing, the lamellar structure could be tough enough to endure the stretching and shearing from the "bridging structure." Without slippage or collapse, the lamellar structure mainly separated through MD, then the perfect slit-like micropore would form between two separated lamellar structure. The lamellar structure' separation with less slippage made the pore structure much more connective, so the pore size and permeability of the microporous membranes increased with the increasing annealing time. From the above results, a model of microstructure changes of annealing was proposed as following. After annealed, the recrystallized lamellae were attached to the both sides of the original lamellae. This structure was like "sandwich" with original lamellae "core" and recrystallized lamellae "shells." These "shells" would improve the ability of preventing from slipping within the original

lamellae. In other words, after the deformation of linear elastic deformation area, the "core–shell sandwich" structure would tend to separate themselves instead of slipping inside of the lamellae. The micropore forming situation was clearly dominated by the microstructure developments during the annealing procedure. As the annealing went on, more micropores with uniform structure were formed during stretching. The micropore structure in Figure 4 was clearly indicated that the "core–shell sandwich" structure formed during annealing had the effect on improving the micropore structure in the stretching procedure.

CONCLUSIONS

1. The chain orientation in crystalline (f_c) region and in amorphous (f_{am}) region and crystallinity (X_c) increased as the annealing time mainly before 200 s specially before 40 s. The increase of f_c, f_{am}, and X_c after 1140 s of annealing were 17%, 14%, and 18% higher than the precursor film.
2. As the annealing time increased, the σ_y and elastic modulus of the annealed films decreased. The shoulder peaks in DSC curves shifted from 141°C to 146°C, and the area of the shoulder peaks grew along the annealing time. This was due to the thickness of the recrystallized lamellae increased as the annealing went on.
3. At the annealing temperature 135°C, the pore size and permeability of the microporous membranes increased with the increasing annealing time. The annealing time more than 480 s was necessary to obtain the better permeability and pore structure of the microporous membranes.
4. The "core–shell sandwich" structure was proposed to explain the microstructure changes during annealing. As the "core–shell sandwich" structure of the lamellar structure was formed during annealing, the feature of tensile deformation properties of annealed films was switched from lamellar slipping to lamellar separation.
5. The pores forming situation of the samples were improved as the annealing time increased. As the annealing went on, the "core–shell sandwich" structure of the lamellar structure improved the ability of slippage resistance in the lamellae; more micropores with uniform structure were formed during stretching.

ACKNOWLEDGMENTS

The authors gratefully acknowledge the financial support of National Natural Science Foundation of China (grant no. 51033003).

REFERENCES

1. Yu, T. H.; Processing and structure-property behavior of microporous polyethylene from resin to final film, Virginia Polytechnic Institute and State University. PhD Thesis **1996**.
2. Zhang, A.; Jiang, H.; Wu, Z.; Wu, C.; Qian, B. *J. Appl. Polym. Sci.* **1991**, *42*, 1779.
3. Yeh, G. S. Y.; Hosemann, R.; Loboda-Čačković, J.; Čačković, H. *Polymer* **1976**, *17*, 309.
4. Arora, P.; Zhang, Z. *Chem. Rev.* **2004**, *104*, 4419.
5. Zhang, S. S. *J. Power Sources* **2007**, *164*, 351.
6. Quynn, G. R.; Brody, H.; Sobering, E. S.; Park, K. K.; Foley, L. R.; *J. Macromol. Sci. B* **1970**, *4*, 953.
7. Sprague, B. S. *J. Macromol. Sci. B* **1973**, *8*, 157.
8. Cannon, S. L.; McKenna, G. B.; Statton, W. O. *J. Polym. Sci. Macromol. Rev.* **1976**, *11*, 209.
9. Wool, R. P. *J. Polym. Sci. Pol. Phys.* **1976**, *14*, 603.
10. Tagawa, T.; Ogura, K. *J. Polym. Sci. Pol. Phys.* **1980**, *18*, 971.
11. Sarada, T.; Sawyer, L. C.; Ostler, M. I. *J. Membr. Sci.* **1983**, *15*, 97.
12. Chou, C. J.; Hiltner, A.; Baer, E. *Polymer* **1986**, *27*, 369.
13. Chen, R. T.; Saw, C. K.; Jamieson, M. G.; Aversa, T. R.; Callahan, R. W. *J. Appl. Polym. Sci.* **1994**, *53*, 471.
14. Yu, T.-H.; Wilkes, G. L. *Polymer* **1996**, *37*, 4675.
15. Sadeghi, F.; Ajji, A.; Carreau, P. J. *Polym. Eng. Sci.* **2007**, *47*, 1170.
16. Sadeghi, F.; Ajji, A.; Carreau, P. J. *J. Membr. Sci.* **2007**, *292*, 62.
17. Sadeghi, F.; Ajji, A.; Carreau, P. J. *J. Polym. Sci. Pol. Phys.* **2008**, *46*, 148.
18. Tabatabaei, S. H.; Carreau, P. J.; Ajji, A. *J. Membr. Sci.* **2008**, *325*, 772.
19. Sadeghi, F.; Tabatabaei, S. H.; Ajji, A.; Carreau, P. J. *J. Polym. Sci. Pol. Phys.* **2009**, *47*, 1219.
20. Tabatabaei, S. H.; Carreau, P. J.; Ajji, A. *J. Membr. Sci.* **2009**, *345*, 148.
21. Tabatabaei, S. H.; Carreau, P. J.; Ajji, A. *Chem. Eng. Sci.* **2009**, *64*, 4719.
22. Ding, Z.; Liu, Z.; Liu, J.; Feng, J.; Yang, W.; Yang, M. *Acta Polym. Sin.* **2012**, 462.
23. Arroyo, M.; Lopez-Manchado, M. A.; Avalos, F. *Polymer* **1997**, *38*, 5587.
24. Somani, R. H.; Hsiao, B. S.; Nogales, A.; Srinivas, S.; Tsou, A. H.; *Macromolecules* **2000**, *33*, 9385.
25. Seki, M.; Thurman, D. W.; Oberhauser, J. P.; Kornfield, J. A. *Macromolecules* **2002**, *35*, 2583.
26. Somani, R. H.; Yang, L.; Hsiao, B. S. *Polymer* **2006**, *47*, 5657.
27. Ferrer-Balas, D.; Maspoch, M. L.; Martinez, A. B.; Santana, O. O. *Polymer* **2001**, *42*, 1697.
28. Mahajan, S. J.; Deopura, B. L.; Wang, Y. M. *J. Appl. Polym. Sci.* **1996**, *60*, 1517.
29. Valles-Lluch, A.; Contat-Rodrigo, L.; Ribes-Greus, A. *J. Appl. Polym. Sci.* **2003**, *89*, 3260.
30. Włochowicz, A.; Eder, M. *Polymer* **1984**, *25*, 1268.
31. Elyashevich, G.; Karpov, E.; Kozlov, A. *Macromol. Symp.* **1999**, *147*, 91.
32. Xanthos, M.; Lin, K. Y.; Sirkar, K. K. *J. Membr. Sci.* **2009**, *330*, 267.
33. Bierenbaum, H. S.; Isaacson, R. B.; Druin, M. L.; Plovan, S. G. *Prod. R&D* **1974**, *13*, 2.
34. Park, I. K.; Noether, H. D. *Colloid Polym. Sci.* **1975**, *253*, 824.
35. Bao, R. Y.; Ding, Z. T.; Zhong, G. J.; Yang, W.; Xie, B. H.; Yang, M. B. *Colloid Polym. Sci.* **2012**, *290*, 261.
36. Uehara, H.; Tamura, T.; Kakiage, M.; Yamanobe, T. *Adv. Funct. Mater.* **2012**, *22*, 2048.